

PAH EMISSION IN THE PROPLYD HST10: WHAT IS THE MECHANISM BEHIND PHOTOEVAPORATION?

S. VICENTE¹, O. BERNÉ^{2,3}, A. G. G. M. TIELENS⁴, N. HUÉLAMO⁵, E. PANTIN⁶, I. KAMP¹, A. CARMONA⁷

Draft version February 12, 2018

ABSTRACT

Proplyds are photodissociation region (PDR)-like cometary cocoons around young stars which are thought to originate through photo-evaporation of the central protoplanetary disk by external UV radiation from the nearby OB stars. This letter presents spatially resolved mid-infrared imaging and spectroscopy of the proplyd HST10 obtained with the VLT/VISIR instrument. These observations allow us to detect Polycyclic Aromatic Hydrocarbons (PAH) emission in the proplyd photodissociation region and to study the general properties of PAHs in proplyds for the first time. We find that PAHs in HST10 are mostly neutral and at least 50 times less abundant than typical values found for the diffuse ISM or the nearby Orion Bar. With such a low PAH abundance, photoelectric heating is significantly reduced. If this low abundance pertains also to the original disk material, gas heating rates could be too low to efficiently drive photoevaporation unless other processes can be identified. Alternatively, the model behind the formation of proplyds as evaporating disks may have to be revised.

Subject headings: circumstellar matter — ISM: lines and bands — protoplanetary disks — stars: individual (HST10) — stars: winds, outflows

1. INTRODUCTION

Most low mass stars are born in transient OB associations (e.g., Lada & Lada 2003), and there is evidence that our own young Solar System evolved near massive stars (e.g., Hester et al. 2004). Externally illuminated protoplanetary disks or *proplyds* (O’Dell et al. 1993) are young stellar objects (YSOs) surrounded by Solar System-sized protoplanetary disks and found embedded within or near a H II region. In these extreme environments the disks are exposed to intense UV radiation fields and stellar winds from the OB stars, dynamical encounters with sibling stars and supernovae, on timescales of planetary system formation and early evolution. Hence, the study of their properties may bring key constraints on the understanding of the general mechanism of planet formation and the origins of our Solar System.

Proplyd morphology has been explained by models of evaporating flows in externally illuminated disks or globules (e.g., Henney et al. 1996; Sutherland 1997; Johnstone et al. 1998; Henney & Arthur 1998; Störzer & Hollenbach 1998, 1999; Richling & Yorke 1998, 2000; Vasconcelos et al. 2011) as a FUV ($6\text{ eV} \leq E < 13.6\text{ eV}$) heated photodissociation region (PDR) encased within a EUV ($E \geq 13.6\text{ eV}$) ionized hydrogen cocoon with a “head-tail” shape. FUV photons of nearby OB stars penetrate deep into the disk and, at relative high column densities, dissociate hydrogen molecules, ionize carbon, and heat the gas to $T \sim 400\text{--}4000\text{ K}$, forming the PDR. The resulting thermal pressure drives an expanding hydrodynam-

ical flow of neutral material escaping from the disk surface with velocities of $1\text{--}3\text{ kms}^{-1}$. The mass-loss rate generated by this photo-evaporation wind determines the lifetime of the gaseous disk and hence the timescale for the formation of giant planets. At some distance from the disk, the EUV photons ionize the neutral wind and form an ionization front (IF) with $T \sim 10^4\text{ K}$. The observed tails result from the diffuse UV radiation field (produced through the recombination of surrounding nebular gas) which drives an evaporation flow on the shadowed side of the disk. These models consider the FUV photoelectric effect on small dust grains and Polycyclic Aromatic Hydrocarbons (PAHs, Joblin & Tielens 2011) as the main gas-heating mechanism at the disk surface. Recent observations (Okada et al., *submitted*) show that PAHs play a major role in the heating process, and theoretical studies (Kamp & Dullemond 2004) confirm this also for protoplanetary disks. The proplyd models mentioned above are adapted from classical PDR models (see Hollenbach & Tielens 1997 for a review) which consider standard interstellar medium (ISM) PAH abundances. However, up to now, there is no observational abundance determination for proplyds.

HST10 (182-413; O’Dell & Wen 1994) is a teardrop-shaped proplyd ($1''.2 \times 2''.6$) containing a prominent nearly edge-on disk ($i \sim 80^\circ$, $PA \sim 86^\circ$) visible as a dark silhouette in H α , optical ionized species and the continuum, but glowing in [OI] $\lambda 6300$ and in the $2.12\text{ }\mu\text{m}$ ro-vibrational line of H₂ (Bally et al. 2000; Chen et al. 1998, Vicente et al., *in prep.*) This object is located at a projected distance of $56''$ from θ^1 Ori C to the SE, the main ionizing star of the Trapezium Cluster ($414 \pm 7\text{ pc}$, Menten et al. 2007). In this letter we present spatially resolved VLT/VISIR observations of PAH emission in HST10. We determine the PAH abundance in the neutral flow and discuss the implications for photo-evaporation models.

2. OBSERVATIONS AND DATA REDUCTION

Mid-IR imaging (75 mas/pix) and low-resolution spectroscopy ($R \sim 200\text{--}350$, 127 mas/pix) of the proplyd HST10 were obtained on the 13th December 2005 with VISIR (Lagage et al. 2004), under good ambient conditions (see-

¹ Kapteyn Astronomical Institute, Postbus 800, 9700 AV, Groningen, The Netherlands

² Université de Toulouse; UPS-OMP; IRAP; Toulouse, France

³ CNRS; IRAP; 9 Av. colonel Roche, BP 44346, F-31028 Toulouse cedex 4, France

⁴ Leiden Observatory, Leiden University, Niels Bohrweg 2, NL-2333 CA Leiden, The Netherlands

⁵ CAB (INTA-CSIC), LAEFF, P.O. Box 78, 28691 Villanueva de la Cañada, Madrid, Spain

⁶ Laboratoire AIM, CEA/DSM - CNRS - Université Paris Diderot, IRFU/SAP, 91191 sur Yvette, France

⁷ UJF-Grenoble 1/CNRS-INSU, Institut de Planétologie et d’Astrophysique de Grenoble (IPAG) UMR 5274, Grenoble, F-38041, France

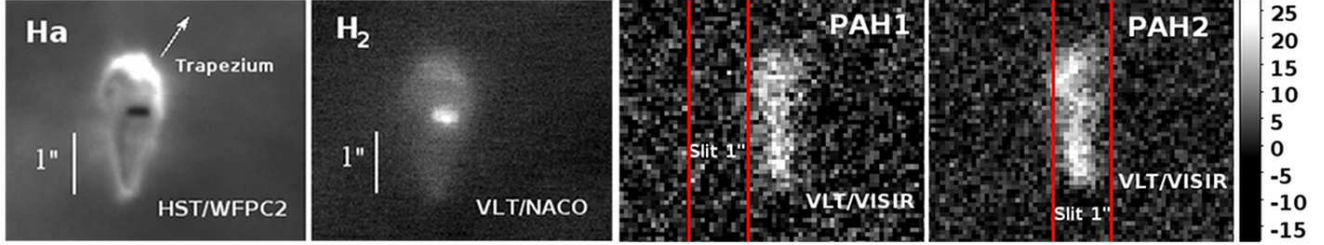


Figure 1. HST10 images (from left to right): $H\alpha$ ($0.656 \mu\text{m}$) from HST/WFPC2 (45.6 mas/pix; HST archive), H_2 ($2.12 \mu\text{m}$) from VLT/NACO (27 mas/pix; Vicente et al., *in prep.*), and PAH1 ($8.6 \mu\text{m}$) and PAH2 ($11.25 \mu\text{m}$) from VLT/VISIR (75 mas/pix; this work). The VISIR images show the $1''$ slit position for the 8.6 and $11.4 \mu\text{m}$ spectral settings respectively with the intensity scale given in $\text{mJy}/\text{arcsec}^2$. The arrow indicates the direction towards θ^1 Ori C, the main ionizing O-star of the Trapezium cluster. North is up and east to the left.

ing at $0.5 \mu\text{m}$ between $0''.6$ and $1''$). A spectro-photometric standard (HD 35536) of similar airmass was observed immediately before and after the science target to allow for telluric absorption correction and calibration. The data were reduced with a VISIR customary pipeline based on IDL scripts (Pantin et al. 2005) and corrected for the background using a multi-resolution inpainting scheme (Pantin 2010). The images were collected with filters PAH1 ($8.59 \pm 0.21 \mu\text{m}$), SIV ($10.49 \pm 0.08 \mu\text{m}$), and PAH2 ($11.25 \pm 0.3 \mu\text{m}$) for a total exposure time (on source) of 30min and using the parallel chopping/nodding jitter mode with a chopping throw of $7''$. The spatial resolution of the final images ($19'' \times 19''$), measured in the only point source in the field, was $0''.35$ for PAH1 and $0''.34$ for PAH2, the latter being diffraction limited and reflecting the improvement in the seeing⁸. HST10 is spatially resolved in the PAH1 and PAH2 images ($0''.97 \times 2''.5$), but not detected in SIV after nebular subtraction. No central star inside the disk is visible in any of the VISIR images (Fig. 1).

The N -band spectroscopy consisted of three settings centered at 8.5, 9.8 and $11.4 \mu\text{m}$ (1h integration time) chosen for covering the $10 \mu\text{m}$ silicate feature and PAH emission bands at 8.6 and $11.25 \mu\text{m}$. The $1''$ slit was placed along the proplyd head-tail, in the NS orientation, and the chop/nod was performed along the slit with a throw of $8''$. The 1D-spectra were extracted by integrating the flux for each wavelength over the spatial extension of the proplyd (~ 17 - 19 pix) in the 2D background subtracted spectra. They show spatially resolved PAH emission at $11.25 \mu\text{m}$ (Fig. 2) but no detection above the noise level at $8.6 \mu\text{m}$. The slit position, estimated using the RA and DEC values from the headers, is overlaid on top of the VISIR images in Fig. 1 and have an uncertainty of $0''.2$ - $0''.3$, corresponding to the accuracy of (small) relative offsets with the VLT. The RA offset of the slit at $8.6 \mu\text{m}$, relative to the proplyd nominal position in O’Dell & Wen (1994), is $0''.6$ - $0''.8$ to the east which leaves the proplyd out of the slit. We believe this was due to errors occurring during the blind offsetting performed to obtain the HST10 spectra. For the $11.4 \mu\text{m}$ setting the proplyd falls almost entirely inside the slit (see Fig. 1).

The H_2 $2.12 \mu\text{m}$ image (27 mas/pix) was collected with the VLT adaptive optics instrument NACO under program ID 076.C-0874 (PI, S. Vicente). This data is described and analyzed in a forthcoming paper (Vicente et al., *in prep.*). The $H\alpha$ $0.656 \mu\text{m}$ image (45.6 mas/pix) from the Hubble Space

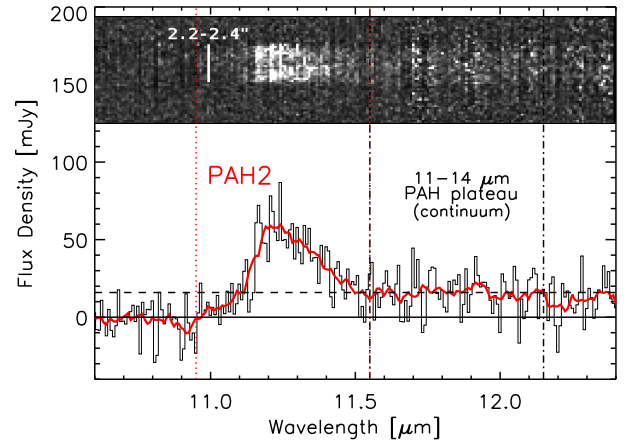


Figure 2. VLT/VISIR low-resolution spectrum ($R \sim 200$) of the proplyd HST10 showing the broad PAH band at $11.25 \mu\text{m}$, and extracted from the 2D spectrum on the top. The PAH2 filter range is indicated by the vertical dotted lines. A flux of 16 mJy for the PAH plateau was determined as the mean flux in an interval of the same length as the PAH2 filter and is represented by the horizontal dashed line. Over-plotted is the spectrum smoothed with a boxcar = 8.

Telescope instrument WFPC2 was retrieved from the ESO archive (program GO 6603, J. Bally). The optical and near-IR images were rebinned to the same pixel size of the VISIR images and aligned with sub-pixel precision (0.01 pix) with IMALIGN/IRAF. The NACO image was used as reference because it contained several point sources in the field, contrary to the VISIR and HST images for which only one to two stars could be found. Although there is a perfect overlap of the centroids of the stars in the RGB image, the estimated error in the alignment is ± 1 pix (or ± 75 mas) from comparison of the position of the silhouette disk seen in the $H\alpha$ image to the H_2 disk emission seen in the NACO image (Fig. 3). This error results from the different Point Spread Functions (PSFs) observed at the different wavelengths ($0''.06$ for $H\alpha$, $0''.08$ for H_2 , and $0''.35$ for PAHs).

3. OBSERVATIONAL RESULTS

Fig. 1 shows the optical, near-IR and mid-IR images of HST10 tracing the different key elements of its morphology. The optical $H\alpha$ image traces the ionized gas at the ionization front with its peak surface brightness facing the Trapezium stars. This is a clear evidence that θ^1 Ori C is the main source of UV radiation driving the photo-ionization and evaporation in HST10. The H_2 $2.12 \mu\text{m}$ emission traces the molecular gas at the disk surface. This was first discovered in a

⁸ The diffraction limit at the VLT (8.2m) varies from $0''.26$ to $0''.34$ in the range $8.6 - 11.25 \mu\text{m}$. As the size of a UT mirror is comparable to the turbulence outer scale, VISIR data are already diffraction limited for optical seeing below $0''.6$.

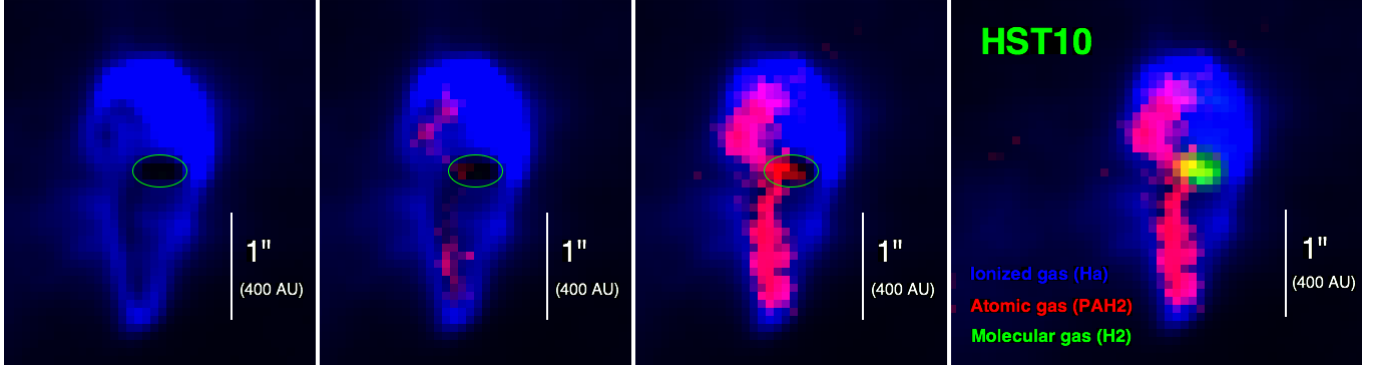


Figure 3. Color composite image of the proplyd HST10 applying a square-root stretch in intensities for better contrast, and showing the different regions traced by the different wavelengths: $H\alpha$ tracing the ionized gas at the ionization front (blue), H_2 the molecular gas at the surface of the nearly edge-on protoplanetary disk (green), and the PAHs emission the atomic gas within the PDR (red). From left to right we increase progressively the intensity of the PAH2 emission and find it to be coincident with the more extinguished or less emitting regions in the $H\alpha$ optical image. The silhouette disk is indicated by the green ellipse.

HST/NICMOS image (Chen et al. 1998) and more recently confirmed with adaptive optics ground-based imaging (Vicente et al., *in prep.*). The VISIR mid-IR images reported here show emission associated to the proplyd in both filters PAH1 ($8.6 \mu\text{m}$) and PAH2 ($11.25 \mu\text{m}$). The latter detection is also confirmed with spectroscopic observations (Fig. 2) and can be attributed to (solo) C-H out-of-plane bending mode in PAH molecules with long straight edges. No continuum is observed below $11 \mu\text{m}$, but beyond $11.3 \mu\text{m}$ we see in Fig. 2 the 11-14 μm PAH plateau resulting from the blend of C-H out-of-plane bending modes (e.g. arising from PAH clusters). On the basis of the similarity of the morphologies in the PAH1 and PAH2 images, and since the PAH1 filter is also situated on top of a C-H vibration (in-plane bending mode), we conclude the PAH1 emission is also due to PAHs. The total density flux integrated over the full proplyd extension (rectangular aperture of 25×45 pix) in the PAH1 image is 26.6 ± 0.5 mJy (3σ) when considering only the photon noise. Given that the uncertainty in the conversion factor used for calibrating the images is typically 10%, we obtain 26.6 ± 2.6 mJy. The integrated flux of the $11.25 \mu\text{m}$ feature in the spectrum, divided by the passband of the PAH2 imaging filter ($10.95 - 11.55 \mu\text{m}$), is 29.4 ± 12.9 mJy (1σ) which is consistent, within the error, with the extracted photometry in the PAH2 image, 38.8 ± 3.8 mJy. The smaller value obtained from the spectrum with respect to imaging is likely due to slit losses which were worsened by pointing inaccuracies from the blind offsetting. The $11.25 \mu\text{m}$ emission observed in the 2D-spectrum in Fig. 2 is extended over ~ 17 - 19 pixels or $2''.2 - 2''.4$ (127 mas/pix), similar to the head-to-tail size of HST10 in the PAH images, and is about 50 mJy at the peak position. The maximum surface brightness in the PAH1 and PAH2 filters ($I_{8.6}$ and $I_{11.25}$) were derived by taking the average of the four brightest pixels at the proplyd head in each VISIR image. These values are given in Table 1.

4. PROPERTIES OF PAHS IN HST10

4.1. Spatial distribution and ionization

In PDRs, PAHs emit mostly in the neutral gas where the majority of molecules are dissociated by FUV photons (e.g. in the nearby Orion Bar, Tielens et al. 1994). Hence, PAHs are a tracer of the atomic gas (for instance in the NGC 7023 nebula they follow the far infrared emission of C^+ , Joblin et al. 2010), and in the particular case of proplyds, PAHs will trace the morphology of the photo-evaporating flow. This is well illustrated in Fig. 3 showing the ionized ($H\alpha$), neutral (PAHs) and molecular (H_2) gas components of the proplyd HST10.

The PAH emission is localized within the ionized envelope and at the disk surface from where, according to PDR models, the FUV-heated material evaporates generating the neutral wind and creating the proplyd PDR. Additionally, even though the PAH1 and PAH2 emission show similar head-to-tail extent, their distribution is different. PAH1 emission at $8.6 \mu\text{m}$ is fainter ($\sim 2\times$ in surface brightness) and more homogeneously distributed within the cocoon, whereas the PAH2 emission at $11.25 \mu\text{m}$ is sharper and brighter on the opposite side to the direction of θ^1 Ori C, and coincident with the areas showing less emission or more heavily extinguished in the optical $H\alpha$ image (Fig. 3). Considering that most of the optical extinction is caused by $\sim 0.1 \mu\text{m}$ dust grains, and these are expected to be depleted in the neutral flow (with $A_V = 0.1 - 0.2$, Henney & O’Dell 1999) due to grain growth and settling in the protoplanetary disk, the $11.25 \mu\text{m}$ emission is tracing the regions of higher density in atomic gas and possibly very small particles of dust. Additionally, while the $11.25 \mu\text{m}$ feature is dominant for neutral PAH molecules, the $8.6 \mu\text{m}$ feature is stronger for ionized PAHs mostly present in high UV irradiated regions (Joblin & Tielens 2011, and references there in). Hence, the difference in spatial distribution observed in the two filters may reflect a charge effect associated to the proplyd location in the foreground of the nebula, that is, in between θ^1 Ori C and the observer. Positively ionized PAHs are expected to be more abundant on the irradiated side of the proplyd opposite to us, whereas the bulk of the PAHs reservoir, as seen in the proplyd “shadowed” side, seem to be in the form of neutral molecules. The $I_{8.6}/I_{11.25}$ band ratio, at the position where we extracted brightnesses in HST10, is of the order of 0.5, in accordance to the astronomical template of Pilleri et al. (2012) for which a value around 0.4 is found for neutral PAHs and 1.45 for PAH^+ . For high radiation fields, PAHs can be neutral if the density of the gas in the flow is high ($\sim 10^6 \text{ cm}^{-3}$, Tielens 2005), allowing for efficient recombination of PAH cations with slow electrons. As we will see, this is most likely the case (Sect. 4.2). Finally, we note that there is no PAH emission beyond the ionization front, suggesting that they are largely destroyed beyond this point as seen in the Orion Bar (Giard et al. 1994).

4.2. PAH abundance

Proplyd models consider disk photoevaporation to be due mainly to efficient heating of the gas by energetic photoelectrons provided by small grains and PAH molecules. However, these models assume PAHs in proplyds are as abundant

Table 1
Parameters of NGC 7023 and HST10 used to derive the PAH abundance in equation 1

Parameter		Reference
NGC 7023		
$I_{8.6}$	$1306 \pm 5 \text{ MJy sr}^{-1}$	this paper
$I_{11.25}$	$2723 \pm 6 \text{ MJy sr}^{-1}$	this paper
G_0	2.6×10^3	Joblin et al. 2010
N_H	$1 \times 10^{22} \text{ cm}^{-2}$	Joblin et al. 2010
f_C^{PAH}	7×10^{-2}	Berné & Tielens 2012
HST 10		
$I_{8.6}$	$720 \pm 111 \text{ MJy sr}^{-1}$	this paper
$I_{11.25}$	$1466 \pm 111 \text{ MJy sr}^{-1}$	this paper
$I_{8.6}/I_{11.25}$	0.5	this paper
G_0	2.4×10^5	Störzer & Hollenbach 1999
N_H	$5.5 \times 10^{21} \text{ cm}^{-2}$	Störzer & Hollenbach 1999
f_C^{PAH}	8×10^{-4}	this paper

as in the interstellar medium (ISM), an assumption which has not yet been verified with observations. PAHs have been detected in, at most, 15% of the observed disks around isolated T Tauri stars and they are under-abundant by a factor of 25 when compared to the ISM (Geers et al. 2007; Oliveira et al. 2010). The VISIR images of HST10 presented in this paper can be used to estimate the abundance of PAHs in a proplyd PDR for the first time.

The mid-IR PAH emission at a given wavelength I_λ is proportional to the number of carbon atoms locked in PAHs in the line of sight (e.g. Joblin et al. 2010), and on the intensity of the UV radiation field, G_0 ⁹. Hence, we can write

$$I_\lambda = \epsilon_\lambda f_C^{PAH} \frac{[C]}{[H]} N_H G_0, \quad (1)$$

where f_C^{PAH} is the fraction of elemental carbon locked in PAHs, N_H is the column density of hydrogen atoms in the line of sight, $[C]/[H]$ is the abundance of carbon relative to hydrogen atoms (1.6×10^{-4}), and ϵ_λ is the PAH emissivity at the given wavelength. The latter parameter, ϵ_λ can be derived for sources where all the other parameters given in Eq. 1 can be determined independently as in the case of the reflection nebula NGC 7023. The values adopted for f_C^{PAH} , N_H and G_0 were taken from the literature (Table 1) while the intensities $I_{8.6}$ and $I_{11.25}$ for NGC 7023 were measured directly in the *Spitzer* IRS spectrum (Pilleri et al. 2012). This yields for the PAH emissivities $\epsilon_{8.6} = 4.5 \times 10^{-18}$ and $\epsilon_{11.25} = 9.4 \times 10^{-18} \text{ MJy sr}^{-1} \text{ cm}^{-2} G_0^{-1}$ which, when inserted in Eq. 1 combined with the parameters in Table 1, give the PAH abundance in the PDR of HST10, f_C^{PAH} , if a good estimate of the column density of atomic gas in the line of sight N_H is provided. This parameter can be estimated from the electron density at the ionization front which can be measured with a fair accuracy. Bally et al. (1998) obtain a value of $n_e = 8 \times 10^4 \text{ cm}^{-3}$ from the $H\alpha$ surface brightness, while Störzer & Hollenbach (1999) find $n_e = 1.1 \times 10^5 \text{ cm}^{-3}$, when

correcting for the extinction to the Orion Nebula. Assuming pressure equilibrium at the ionization front, the density of H atoms in the neutral flow n_H , must be of the order of $10 \times n_e$ or $n_H \sim 10^6 \text{ cm}^{-3}$. For a head width of $\sim 6 \times 10^{15} \text{ cm}$, measured in the PAH2 image, and assuming this value for the neutral flow length along the line of sight (symmetry in HST10), we obtain $N_H \sim 6 \times 10^{21} \text{ cm}^{-2}$. From models and using the same parameters, Störzer & Hollenbach (1999) find $N_H = 5.5 \times 10^{21} \text{ cm}^{-2}$. Adopting their value for N_H , and using the brightnesses $I_{8.6}$ and $I_{11.25}$ (Table 1) measured in the VISIR PAH1 and PAH2 images, we find similar PAH abundances in HST10 of $f_C^{PAH} = 8.1 \times 10^{-4}$ and $f_C^{PAH} = 8.0 \times 10^{-4}$. These values are nevertheless extremely low: they correspond to an abundance of PAHs 90 times lower than in NGC 7023 (Berné & Tielens 2012), or about 50 times less than the values found in the Orion Bar or in the diffuse ISM (Tielens 2005). And, since the brightnesses I_λ have been measured for the brightest pixels at the proplyd head (Sect. 3), our estimation gives the maximum abundance of PAHs in the evaporating flow toward θ^1 Ori C.

5. DISCUSSION

As other studies of T Tauri stars (Geers et al. 2007; Oliveira et al. 2010) we find PAHs to be under-abundant in the PDR of the proplyd HST10, by a factor of 50 or more relative to the diffuse ISM. The origin of this under-abundance cannot be readily explained, but some proposed hypotheses include clustering of PAHs followed by sedimentation inside the disk, destruction by FUV photons in the PDR, or destruction by X-rays emitted by the low-mass central star¹⁰. Nevertheless, more important than the causes for PAH under-abundance are the implications this result has on our understanding of the physical processes shaping morphology and driving mass-loss in proplyds. Photo-evaporation of proplyds has been explained so far by the photo-electric heating of the gas which is known to have a much reduced photo-electric efficiency for grains larger than 100 \AA (Tielens 2005). Given the high column density $N_H = 5.5 \times 10^{21} \text{ cm}^{-2}$ and low extinction $A_V = 0.1 - 0.2$ in the PDR of HST10, we expect these large grains to be depleted in the neutral flow. In fact, the photoelectric heating has its highest efficiency for PAHs (molecules of a few Å) and the small end of the very small grains (up to a few tens of Å). But according to Pilleri et al. (2012) (Fig. 6 in their paper), for high radiation fields as those found in proplyds ($> 10^4 G_0$), the very small grains are destroyed and evaporated into free-flying PAHs. Therefore, we do expect PAHs to be the main agents of the photo-electric heating in proplyds.

Assuming the disk surface has the same PAH abundance as the proplyd PDR (they are lifted from the disk surface by the evaporative wind), the low fraction of PAHs found in this letter will have a profound impact on the disk surface gas temperature. And hence, the current hypothesis of an evaporating disk creating the proplyd PDR and morphology may have to be revised. Two possibilities arise: 1) other gas heating mechanisms are relevant for disk evaporation, such as collisional de-excitation of UV pumped H_2 and H_2 photo-dissociation followed by reformation on grain surfaces; 2) the PAH emission from the proplyd cocoon is associated to remnant atomic gas from the protostellar envelope or the surrounding nebula. By combining detailed modeling with upcoming Her-

⁹ expressed in terms of the Habing field which corresponds to an integrated intensity between 91.2 and 240nm of $1.6 \times 10^{-3} \text{ ergs cm}^{-2} \text{ s}^{-1}$ (Habing 1968).

¹⁰ The majority of stars in the Orion Nebula cluster are in the mass range of $0.1 - 1.5 M_\odot$ (Hillenbrand & Hartmann 1998)

schel (Berné et al., *in prep.*) and VLT data (Vicente et al., *in prep.*), the heating-cooling mechanisms at the disk surface can be assessed allowing to test each one of the possible scenarios creating the puzzling proplyd morphology.

REFERENCES

- Bally, J., Sutherland, R. S., Devine, D., & Johnstone, D. 1998, *AJ*, 116, 293
 Bally, J., O'Dell, C. R., & McCaughrean, M. J. 2000, *AJ*, 119, 2919
 Berné, O., & Tielens, A. G. G. M. 2012, *Proceedings of the National Academy of Science*, 109, 401
 Chen, H., Bally, J., O'Dell, C. R., et al. 1998, *ApJ*, 492, L173
 Geers, V. C., van Dishoeck, E. F., Visser, R., et al. 2007, *A&A*, 476, 279
 Giard, M., Bernard, J. P., Lacombe, F., Normand, P., & Rouan, D. 1994, *A&A*, 291, 239
 Habing, H. J. 1968, *Bull. Astron. Inst. Netherlands*, 19, 421
 Henney, W. J., Raga, A. C., Lizano, S., & Curiel, S. 1996, *ApJ*, 465, 216
 Henney, W. J., & Arthur, S. J. 1998, *AJ*, 116, 322
 Henney, W. J., & O'Dell, C. R. 1999, *AJ*, 118, 2350
 Hester, J. J., Desch, S. J., Healy, K. R., & Leshin, L. A. 2004, *Science*, 304, 1116
 Hillenbrand, L. A., & Hartmann, L. W. 1998, *ApJ*, 492, 540
 Hollenbach, D. J., & Tielens, A. G. G. M. 1997, *ARA&A*, 35, 179
 Joblin, C., Pilleri, P., Montillaud, J., et al. 2010, *A&A*, 521, L25
 Joblin, C., & Tielens, A. G. G. M. 2011, *EAS Publications Series*, 46, Johnstone, D., Hollenbach, D., & Bally, J. 1998, *ApJ*, 499, 758
 Kamp, I., & Dullemond, C. P. 2004, *ApJ*, 615, 991
 Lada, C. J., & Lada, E. A. 2003, *ARA&A*, 41, 57
 Lada, C. J., Muench, A. A., Lada, E. A., & Alves, J. F. 2004, *AJ*, 128, 1254
 Lagage, P. O., Pel, J. W., Authier, M., et al. 2004, *The Messenger*, 117, 12
 Menten, K. M., Reid, M. J., Forbrich, J., & Brunthaler, A. 2007, *A&A*, 474, 515
 O'Dell, C. R., Wen, Z., & Hu, X. 1993, *ApJ*, 410, 696
 O'Dell, C. R., & Wen, Z. 1994, *ApJ*, 436, 194
 Oliveira, I., Pontoppidan, K. M., Merín, B., et al. 2010, *ApJ*, 714, 778
 Pantin, E., Lagage, O.-P., Claret, A., et al. 2005, *The Messenger*, 119, 25
 Pantin, E. 2010, Ph.D. Thesis, *Infrared Observations of Circumstellar Disks and Exoplanets*, Université de Paris Diderot, 2010
 Pilleri, P., Montillaud, J., Berné, O., & Joblin, C. 2012, *A&A*, 542, A69
 Richling, S., & Yorke, H. W. 1998, *A&A*, 340, 508
 Richling, S., & Yorke, H. W. 2000, *ApJ*, 539, 258
 Störzer, H., & Hollenbach, D. 1998, *ApJ*, 495, 853
 Störzer, H., & Hollenbach, D. 1999, *ApJ*, 515, 669
 Sutherland, R. S. 1997, *IAU Colloq. 163: Accretion Phenomena and Related Outflows*, 121, 566
 Tielens, A. G. G. M., McKee, C. F., Seab, C. G., & Hollenbach, D. J. 1994, *ApJ*, 431, 321
 Tielens, A. G. G. M. 2005, *The Physics and Chemistry of the Interstellar Medium*, by A. G. G. M. Tielens, pp. . ISBN 0521826349. Cambridge, UK: Cambridge University Press, 2005
 Vasconcelos, M. J., Cerqueira, A. H., & Raga, A. C. 2011, *A&A*, 527, A86